 CMC, vol.17, no.3, pp.215-232, 2010

Nanostiffening in Polymeric Nanocomposites

J. Wang[1] and D. C. C. Lam[2]

Abstract: Selected elastic moduli of nanocomposites are higher than the elastic moduli of microcomposites. Molecular immobilization and crystallization at the interfaces had been proposed as potential causes, but studies suggested that these effects are minor and cannot be used to explain the magnitude observed in nanocomposites with >3nm particles. Alternately, molecular simulation of polymer deformation showed that rotation gradients can lead to additional molecular rotations and stiffen the matrix. The stiffening is characterized by the nanostiffening material parameter, l_2. In this investigation, an analytical expression for nanostiffening in nanocomposites was developed using finite element analysis. The nanostiffening in nanocomposites was determined by the ratio of l_2 to the particle size r, and the expression was shown to be in good agreement with experimental data from the literature. The dependence on the ratio suggests that nanostiffening is significant only for nanocomposites with large l_2/r but is negligible when l_2/r is small.

Keywords: Size stiffening, Nanocomposite, Polymer, Strain gradient, Modeling.

1 Introduction

Composites are traditionally reinforced with micron-sized inclusions (Verbeek, 2003; Spanoudakis and Young, 1984; Radford, 1971). Models of elastic modulus of microcomposites (Kerner, 1956; Tucker and Liang, 1999) have been reviewed by Fu et al. (2008) and are summarized in appendix A. These micromechanics models rely on the idea that the effective elastic modulus of composite materials are functions of the properties of the constituents, volume fraction of components, shape and arrangement of inclusions, and the matrix-inclusion interface. Amongst these models, the semi-empirical Halpin-Tsai's equation (Halpin, 1969; Halpin and Tsai, 1969) has been shown to compare well with experimental data. The equation can

[1] Fudan University, Shanghai 200433, PR-China

[2] The Hong Kong University of Science and Technology, Clear Water Bay, Kowloon, HONG KONG, Corresponding Author: Email: david.lam@ust.hk

be written as

$$\frac{E_{co}}{E_m} = \frac{1+\xi\eta\varphi_p}{1-\eta\varphi_p}. \tag{1}$$

where, φ_p is the particle volume fraction and E_{co}, E_p and E_m are the elastic moduli of the composites, particle and matrix, respectively. η and ξ are constants of polymer composites. η is an elastic parameter,

$$\eta = \frac{(E_p/E_m)-1}{(E_p/E_m)+1}. \tag{2}$$

ξ in Eq. (1) is equal to 2 for spherical particles, but is, in general, a parameter dependent on the particle shape and the matrix Poisson's ratio. Halpin-Tsai's model and similar models in Appendix A were developed using strain-based mechanics and are *independent of particle size*.

Recently, processing techniques have been developed to allow the size of inclusions to go down to nanoscale. Experiments have shown that nanoscale reinforcement brings new phenomena, which contribute to material properties. When nanoparticles were added, the elastic modulus of the nanocomposite became size-dependent. When Meinecke and Taftaf (1988) added 22v% of nanocarbon to Styrene-Butadiene-Rubber (SBR), the normalized elastic modulus, E_c/E_m increased to > 4, where E_c is the elastic modulus of nanoparticulate-reinforced composite. Others added 4v% of nanoclay into nylon 6 which increased E_c/E_m to 2.65 (Ji et al., 2002). Similarly, addition of 2v% of 39 nm $CaCO_3$ crystal particles into polypropylene increased E_c/E_m 3 folds (Mishra et al., 2005). When smaller 21 nm $CaCO_3$ particles were added at the same volume fraction, E_c/E_m increased to >4.5. When nanoparticles are added, the amount of increase in E_c is significantly higher than the conventional E_{co} and these behaviors cannot be explained by the strain-based models in the appendix A.

In general, rotation gradients are ignored in strain-based models such that the stiffening is independent of the particle size. Contributions from rotation gradients in the matrix can be ignored because the amount of particle/matrix interfaces is small in microcomposites. In nanocomposites, the particle/matrix interfacial area is increased by more than 100 folds and the rotation gradients in the surrounding interfacial regions can no longer be ignored. Rotation gradients in polymers generate additional molecular rotations in the polymers and increase the deformation energy of the solid (see appendix B). On this basis, we developed a finite element model with rotation gradients to describe the stiffening in nanocomposites. An analytical expression developed from the results was found to successfully explain nanocomposite stiffening behavior previously unexplained by conventional theory.

2 Methodology

2.1 Deformation energy

Conventional finite element analysis calculates the deformation energy using strain-based elasticity. The deformation energy density w in strain-based elasticity is

$$w = \frac{1}{2}k\varepsilon_{ii}\varepsilon_{jj} + \mu\varepsilon'_{ij}\varepsilon'_{ij}, \tag{3}$$

where, ε'_{ij} is deviatoric strain,

$$\varepsilon'_{ij} = \varepsilon_{ij} - \frac{1}{3}\varepsilon_{mm}\delta_{ij}. \tag{4}$$

k and μ are bulk and shear moduli respectively. Strain gradients can be included in the deformation energy by using the higher-order deformation energy density, w^h,

$$w^h = w^h\left(\varepsilon_{ij}, \eta_{ijk}\right), \tag{5}$$

where $\eta_{ijk} = \partial_{ij}u_k$ is the strain gradient tensor, and ∂_i is the forward gradient operator. By regrouping the invariant of strain gradient tensor and introducing the equilibrium equation of moment of couples (Yang et al., 2002), the deformation energy density with higher-order terms is

$$w^h = w^h\left(\varepsilon_{ij}, \gamma_i, \eta^{(1)}_{ijk}, \chi^s_{ij}\right), \tag{6}$$

where, γ_i, $\eta^{(1)}_{ijk}$ and χ^s_{ij} are the dilatation gradient vector, the deviatoric stretch gradient tensor and the symmetric rotation gradient tensor respectively (Lam et al., 2003). For polymers, only rotation gradients are mechanistically defined (Nikolov et al., 2007). Hence, the deformation energy density with higher-order terms for polymers is

$$w^h = \frac{1}{2}k\varepsilon_{ii}\varepsilon_{jj} + \mu\varepsilon'_{ij}\varepsilon'_{ij} + \mu l_2^2\chi^s_{ij}\chi^s_{ij}, \tag{7}$$

where, l_2 is the higher-order material nanostiffening material parameter associated with symmetric rotation gradient χ^s_{ij}. l_2 of the material and χ^s_{ij} in the matrix will determine degree of nanostiffening.

2.2 Modeling approach

When the strain gradients are involved, the C^1-continuity is generally required for displacement interpolation, and is a well known difficulty in displacement-based finite element method. To overcome the difficulty, the mixed-type finite element formulation was developed to model strain gradients behaviors (Amanatidou and Aravas, 2002; Shu et al., 1999). Though the mix-type elements were implemented successfully to account for strain gradient effects, the formulation is complex and the solution is heuristically dependent on the specific nature of the problem in numerical analysis.

Instead of approaching higher-order mechanics with this complex formulation, examination of the physical character of higher-order behavior can assist in the development of an alternative approach to the higher-order modeling. According to the strain gradient elasticity analysis by Wang and Lam (2009), the conventional displacement field that satisfies the governing equations in strain-based mechanics also satisfies the higher-order governing equations in the domain. This means that the higher-order solution and the conventional solution share the same displacement field everywhere except on the boundaries. Furthermore, the higher-order effect at the boundary was shown to be minor (Lam et al, 2003). On the basis of this template approach, the classical displacement field can be used as template and the strain gradients and the corresponding higher-order stresses can be computed by selecting appropriate C^0 shape function. The applicability of conventional displacement field for use as a template field in higher-order beam bending and micro-rod torsion was examined by Wang and Lam (2009). The results were benchmarked with strain gradient analytical solutions and experimental results, and good agreements were obtained (Appendix C). A similar approach, conventional displacement template, was used to develop strain gradient plastic element with C^0 shape function (Swaddiwudhipong S. et al, 2005). The method was used to analyze higher-order indentation and the results were in good agreement with experiments (Swaddiwudhipong S. et al, 2005). Similar approach was also used by Askes et al. (2008) for higher-order analysis using classical un-regrouped strain gradients.

In this investigation, the conventional displacement field from strain-based FEM was used as the template field. Both the strain and strain gradient field can be obtained by differentiating the displacement field continuously, and the deformation energy density was computed according to Eq. (7). The total deformation energy was obtained by integrating the deformation energy density over the whole volume. The external force was then determined by differentiating the total elastic deformation energy with respect to the displacements at the loading point.

To incorporate the rotation gradients into the finite element model, the formulation

on the discrete element level is needed. In an arbitrary element, the displacement can be expressed as

$$u_i = \sum_{n=1}^{M} N_n q_i^n. \tag{8}$$

Where, u_i denotes displacement component, N_n is the shape function of node n, M is the number of element node, and q_i^n is the nodal displacement component value of node n. The strain is

$$\varepsilon_{ij} = \frac{1}{2} \sum_{n=1}^{M} \left[q_i^n \left(\nabla_j N_n \right) + \left(\nabla_i N_n \right) q_j^n \right] \tag{9}$$

and the strain gradient is

$$\eta_{ijk} = \sum_{n=1}^{M} \left[\nabla_i \left(\nabla_j N_n \right) \right] q_k^n, \tag{10}$$

where, ∇_i is the gradient operator, and the components of rotation gradients χ_{ij}^s can be calculated from η_{ijk}. Then the deformation energy in the element is

$$w^e = \int_{V^e} \left[\frac{1}{2} k \varepsilon_{ii} \varepsilon_{jj} + \mu \left(\varepsilon'_{ij} \varepsilon'_{ij} + l_2^2 \chi_{ij}^s \chi_{ij}^s \right) \right] dV, \tag{11}$$

which is obtained using the Gaussian numerical integration. The total deformation energy of the structure is the sum of the energies in all elements,

$$W = \sum_{s=1}^{L} w^e, \tag{12}$$

where L denotes the total element number in the structure, and the external force vector is

$$\mathbf{F} = \frac{\partial W}{\partial \mathbf{u}}. \tag{13}$$

In the case of a bar, the effective elastic modulus of the structure is then determined from $\boldsymbol{F}$ and bar displacements at $\boldsymbol{F}$.

3 Modeling of particulate-reinforced composite

The elastic modulus of a bar in tension can be determined using FEM. Addition of particles in a simple cubic arrangement (Fig. 1) into the polymer increases the elastic modulus of the unit cell. From the unit cell, a bar in tension can be generated by repeating the unit cell in space and the volume fraction of particles is controlled by the ratio of particle size and unit cell length within a cell.

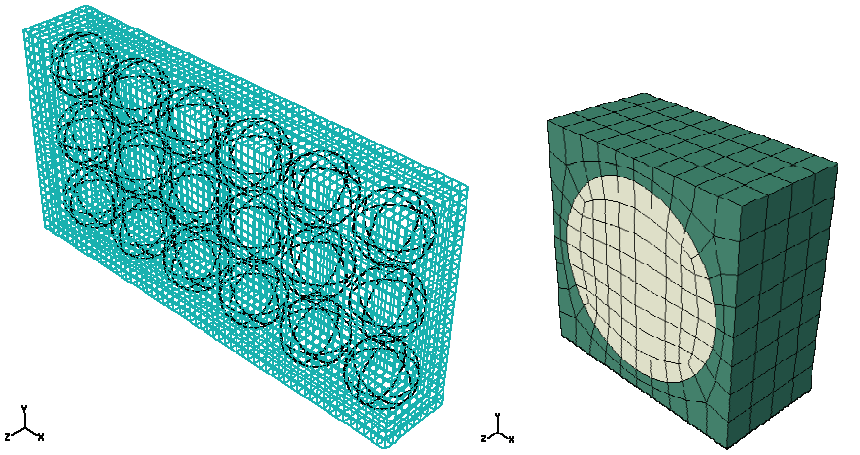

(a) whole meshes (b) SC half unit cell mesh

Figure 1: The meshes for simple cubic (SC) arrangement of the particles in a bar.

3.1 Tension stiffening

When the composite bar is loaded in tension, the matrix near the hard particles has high rotation gradients. The contour and profile of the rotation gradient product, $g_{rot} = \chi^s_{ij}\chi^s_{ij}$ in a bar with 15v% of particles are shown in Fig. 2. The profile in Fig. 2(b) shows g_{rot} near the particles increases with E_p/E_m, but becomes asymptotic when E_p/E_m is 100.

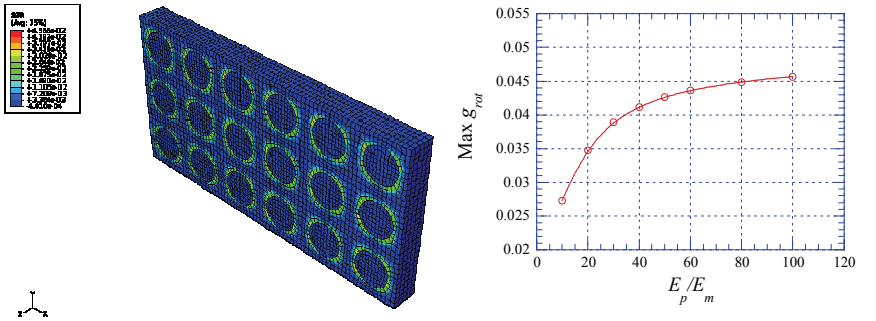

(a) E_p/E_m=100 (b) Local maximum g_{rot} vs. E_p/E_m

Figure 2: Contour and profiles of g_{rot} for SC pattern composite when $\varphi_p = 15\%$.

The composite elastic modulus ratio (E_c/E_{co}) is plotted as a function of the particle radius r (Fig. 3) for constant E_p/E_m. At constant volume fraction, E_c/E_{co} is independent of the particle size, but increases when φ_p is increased from 10v% to 20v%. When rotation gradients are included (Fig. 3), E_c/E_{co} becomes *size-dependent* when the particle size is small.

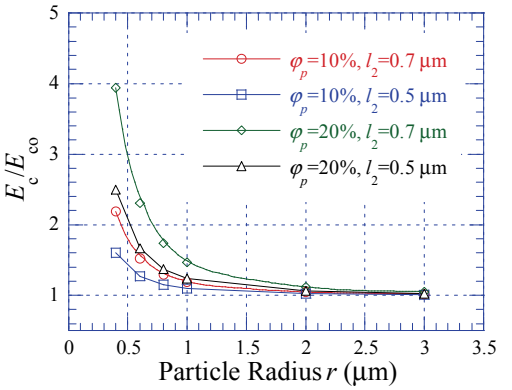

Figure 3: The normalized composite tensile modulus E_c/E_{co} as a function of the particle size.

In general, the particle surface area increases with the inverse square of the particle radius r, and E_c/E_{co} can be plotted as an inverse function of r^2 to examine if rotation gradient stiffening is proportional to the particle surface area (Fig. 4). Since the surface area increases linearly with the particle volume fraction φ_p, re-plotting the data with volume fraction showed that the data from composites with different volume fractions and particle sizes collapsed onto a single curve (Fig. 5). The emergence of a single curve suggests that nanostiffening is proportional to the surface area of the particles.

In addition to the surface area dependence, the magnitude of the rotation gradients in the matrix surrounding the particle, g_{rot}, is determined by the particle arrangement and E_p/E_m. g_{rot} vanishes when $E_p = E_m$ (Fig. 2), and correspondingly, E_c/E_{co} is flat when $E_p = E_m$(Fig. 6). The dependence can be modeled using an asymptotic function, $(1\text{-}E_m/E_p)^\beta$. Finite element analyses were conducted for composites with particles arranged in simple cubic (SC), face-centered cubic (FCC) and body center cubic (BCC) configurations (Fig. 7). The data for the composites with different arrangement collapsed onto a single master curve where φ_c is the maximum packing fraction for different particle arrangement. The master curve

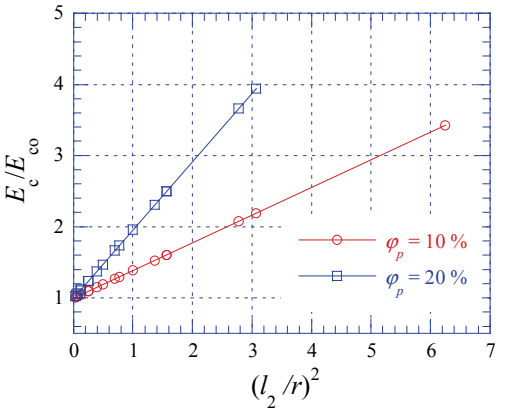

Figure 4: E_c/E_{co} versus $(l_2/r)^2$ for different volume fraction of particles.

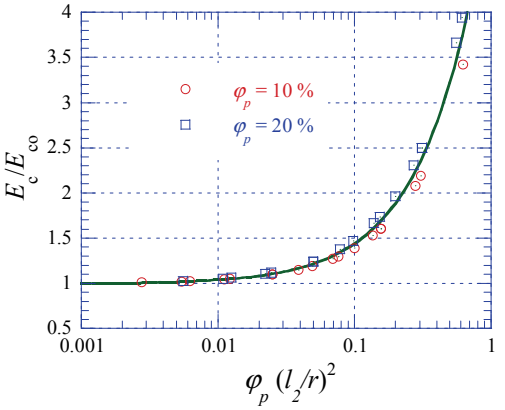

Figure 5: E_c/E_{co} versus $\varphi_p\,(l_2/r)^2$ for different volume fraction of particles.

can be described by the master function,

$$\frac{E_c}{E_{co}} = 1 + \alpha \frac{\varphi_p}{\varphi_c} \left(\frac{l_2}{r}\right)^2 \left(1 - \sqrt{\frac{E_m}{E_p}}\right)^{\beta}, \tag{14}$$

where, $\alpha = 10^{0.6}$ and $\beta = 1.6$ are particle packing constants for the master curve. When the Halpin-Tsai's model is substituted in for E_{co}, the nanostiffened elastic

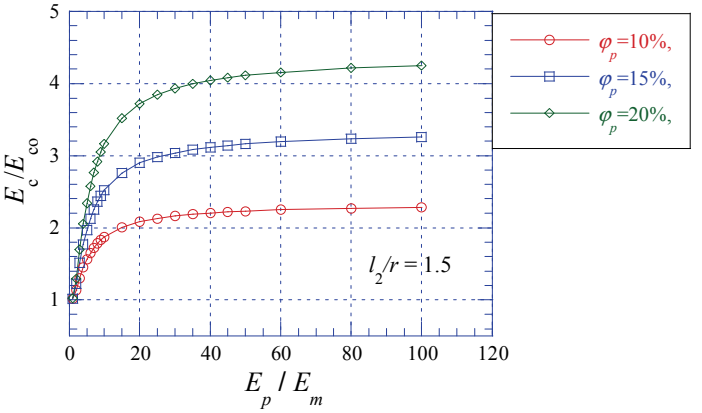

Figure 6: E_c/E_{co} versus E_p/E_m for different volume fraction of particles.

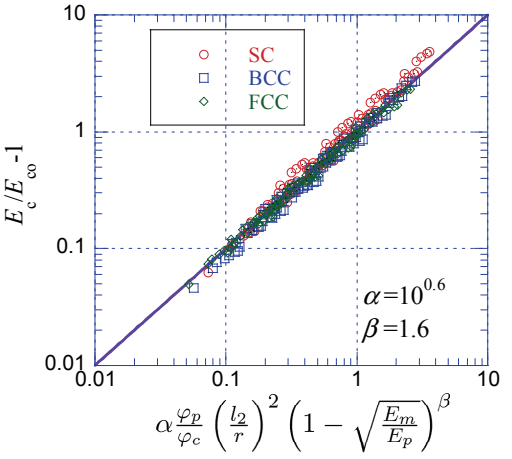

Figure 7: $E_c/E_{co} - 1$ as a function of master curve normalized variable for three particle arrangements.

modulus for nanocomposites becomes,

$$\frac{E_c}{E_m} = \frac{1+\xi\eta\varphi_p}{1-\eta\varphi_p}\left[1+\alpha\frac{\varphi_p}{\varphi_c}\left(\frac{l_2}{r}\right)^2\left(1-\sqrt{\frac{E_m}{E_p}}\right)^\beta\right]. \tag{15}$$

When the matrix's l_2 is small relative to the particle size, nanostiffening is negligible and the nanocomposite elastic modulus reverts back to the Halpin-Tsai's

relation.

3.2 Analysis

Nanocomposites with small l_2/r will not have any significant nanostiffening. Meinecke and Taftaf (1988) studied the elastic modulus of carbon black (50nm; E=9.83 GPa; $\nu = 0.3$) filled rubber composite (E =0.23 GPa; ν =0.49). Comparison of Meinecke and Taftaf's data with the Halpin-Tsai's model (Fig. 8) showed that experimental nanocomposites elastic modulus is significantly higher than the Halpin-Tsai's model and other models in appendix A. Using l_2 = 43 nm, Eq. (15) is plotted as a solid line in Fig. 8, and good agreement is obtained between data and the nanostiffening equation. This suggests that the SBR matrix is strain-stiffened by the hard particles, but also nanostiffened by the rotation gradients in the matrix.

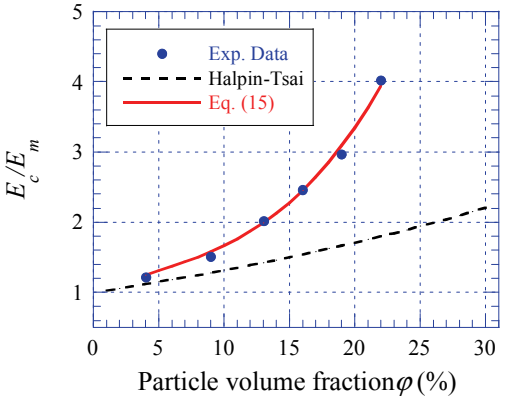

Figure 8: Comparison of conventional strain-based Halpin-Tsai's model to experimental nanocomposite data from Meinecke and Taftaf (1988). The nanostiffening model in Eq. (15) is plotted as a solid line.

4 Discussion

Alternate explanations for the increase in the nanocomposite elastic modulus beyond conventional expectations had been proposed. Chief amongst them is the idea that the macromolecules next to the particles are surface absorbed and are immobilized (Schadler, 2007). Once immobilized, the volume of the particles is effectively increased resulting in an increase of the nanocomposite elastic modulus. Dekkers and Heikens (1983) chemically modified the interfacial adhesion between glass and polystyrene and measured the elastic modulus of the composites. The experimental

results showed that weakening or strengthening the interface has little effect on the composite elastic modulus. Crystallization of the matrix at the interface can also increase the composite elastic modulus. Wang et al. (2003) studied the effect of matrix crystallization and found that the composite elastic modulus increased with crystallization, but the increase is small and cannot be used to explain the behavior observed in nanocomposites.

Strain gradient theories had been used to quantitatively explain size dependent behavior in polymers (Lam et al., 2003; Wang and Lam, 2009). In this study, the nanostiffening relation developed in this study was shown to agree with SBR nanocomposite (r = 50nm) using $l_2 \sim 43$ nm for the matrix. If the l_2, is 1 nm instead, l_2/r would be negligible and nanostiffening would be negligible. Thus, not all nanocomposites are nanostiffened if they are not paired with a proper matrix. l_2 is a function of the chemistry and is dependent on the manner in which the macromolecules are arranged in the solid. The relations between network structure and l_2 are investigated in a companion paper (Wei and Lam, 2010).

5 Remarks

An alternative to the template method would be the meshless approach. The template method fulfills the higher-order governing equation, but requires the relaxation of the C^1 continuity requirements for strain gradients in the finite element formulation to accommodate higher order boundary conditions at the non-free boundary. Alternate mixed formulation can decrease the C^1 continuity to C^0 continuity, but incorporation of the rotation or other gradient of displacement terms in the formulation would result in increase the nodal degree of freedom and make the formulation cumbersome. Instead of using mixed formulations, the meshless approach maybe a better approach to satisfy C^1 continuity. Conventional nodal displacements are used in the meshless approach and C^1 continuity is uncomplicated and straight forward. The continuity of strain gradients in meshless is resolved via the use of interpolation such as that pioneered in the Meshless Local Petrov-Galerkin (MLPG) method (Atluri and Zhu, 1998a and b). The method was shown to have passed the patch test and agreed with analytical solutions in 2D cases (Tang et al (2003)). For general strain gradient materials, MLPG is significantly more computationally intensive than the template method, but for polymers where only rotation gradients are involved, the computational cost would be lower. In general, the template approach is straightforward, efficient and easy to use as a first model for quick results. The MLPG method maybe used to develop a follow-on model when higher precision is required.

6 Conclusions

Additional molecular rotations induced by rotation gradients and characterized by the nanostiffening material parameter l_2 were incorporated in model to investigate the elastic behavior of particulate reinforced composites. The composite elastic moduli of nanostiffened composites were found to increase with the surface area of the particles. A master relation was developed and comparison of the relation and elastic modulus data from nanocarbon reinforced composites using $l_2 \sim$43 nm gave good agreement. The agreement suggests that additional molecular rotations needed to accommodate the rotation gradients in the matrix around the rigid particles is the mechanism underpinning the multi-fold elastic properties increase in nanocomposites.

Acknowledgement: The project is supported by grants from the Research Grant Council (615505 and 615007) of the Hong Kong SAR, China.

References

Amanatidou, E., Aravas, N. (2002): Mixed finite element formulations of strain-gradient elasticity problems. *Comput. Methods Appl. Mech. Eng.*, vol. 191, pp. 1723-1751.

Askes, H., Morata, I., Aifantis, E. C. (2008): Finite element analysis with staggered gradient elasticity. *Comput. Struct.*, vol. 86, pp. 1266-1279.

Atluri, S.N. Zhu, T. (1998a): A new meshless local Petrov-Galerkin (MLPG) approach to nonlinear problems in com-putational modeling and simulation. *Comput. Modeling Simulation in Engrg.* 3: 187-196

Atluri, S.N. Zhu, T. (1998b): A new meshless localPetrov-Galerkin (MLPG) approach in computational mechanics. *Comput. Mech.* 22: 117-127

Coran, A. Y. (2000): Thermoplastic elastomeric rubber – plastic blends. **In: Bhowmick, A. K. and Stephens, H.** (Eds.), *Handbook of Elastomers*, Second Edition. CRC, New York, pp. 265 - 320.

Counto, U. J. (1964): Effect of elastic modulus, creep and creep recovery of concrete. *Mag. Concrete. Res.* vol. 16, pp. 129-138.

Dekkers, M. E. J., Heikens, D. (1983): The effect of interfacial adhesion on the tensile behavior of polystyrene-glass-bead composites. *J. Appl. Polym. Sci.* vol. 28, pp. 3809-3815.

Einstein, A., Fürth, R. (1956): *Investigations on the theory of the Brownian movement*. Dover Publications, New York.

Fu, S.-Y., Feng, X.-Q., Lauke, B., Mai, Y.-W. (2008): Effects of particle size,

particle/matrix interface adhesion and particle loading on mechanical properties of particulate-polymer composites. *Compos. Part B-Eng.*, vol. 39, pp. 933-961.

Guth, E. (1945): Theory of Filler Reinforcement. *J. Appl. Phys.* vol. 16, pp. 20-25.

Halpin, J. C. (1969): Stiffness and expansion estimates for oriented short fiber composites. *J. Compos. Mater.*, vol. 3, pp. 732 -734.

Halpin, J. C., Tsai S. W. (1969): Effects of environmental factors on composite materials. *Technical Report. AFML-TR* pp. 67-423.

Ji, X. L., Jing, J. K., Jiang, W., Jiang, B. Z. (2002): Tensile modulus of polymer nanocomposites. *Polym. Eng. Sci.*, vol. 42, pp. 983-993.

Kerner, E. H. (1956): The elastic and thermoelastic properties of composite media. *Proc. Phys. Soc. London*, pp. 808-813.

Lam, D. C. C., Yang, F., Chong, A. C. M., Wang, J., Tong, P. (2003): Experiments and theory in strain gradient elasticity. *J. Mech. Phys. Solids*, vol. 51, pp. 1477-1508.

Meinecke, E. A., Taftaf, M. I. (1988): Effect of carbon black on the mechanical properties of elastomers. *Rubber Chem. Technol.* vol. 61, pp. 534-547.

Mishra, S., Sonawane, S. H., Singh, R. P. (2005): Studies on characterization of nano $CaCO_3$ prepared by the in situ deposition technique and its application in PP-nano $CaCO_3$ composites. *J. Polym. Sci. Pol. Phys.*, vol 43, pp. 107-113.

Nikolov, S., Han, C. S., Raabe, D. (2007). On the origin of size effects in small-strain elasticity of solid polymers. *Int. J. Solids Struct.*, vol. 44, pp. 1582-1592.

Radford, K. C. (1971): The mechanical properties of an epoxy resin with a second phase dispersion. *J. Mater. Sci.*, vol. 6, pp. 1286-1291.

Schadler, L. (2007): Nanocomposites - Model interfaces. *Nat. Mater.*, vol. 6, pp. 257-258.

Shu, J. Y., King, W. E., Fleck, N. A. (1999): Finite elements for materials with strain gradient effects. *Int. J. Numer. Meth. Eng.*, vol. 44, pp. 373-391.

Spanoudakis, J., Young, R. J. (1984): Crack propagation in a glass particle-filled epoxy resin. *J. Mater. Sci.*, vol. 19, 473-486.

Swaddiwudhipong, S., Hua, J., Tho, K. K., Liu Z. S. (2005): C^0 solid elements for materials with strain gradient effects. *Int. J. Numer. Meth. Eng.*, vol. 64, pp. 1400-1414.

Swaddiwudhipong, S., Poh L. H., Hua, J., Liu Z. S., Tho K. K. (2005): Modeling nano-indentation tests of glassy polymers using finite elements with strain gradient plasticity. *Mater. Sci. .Eng. A*, vol. 404, pp. 179–187.

Tucker Iii, C. L., Liang, E. (1999): Stiffness predictions for unidirectional short-fiber composites: Review and evaluation. *Compos. Sci. Technol.*, vol. 59, pp. 655-671.

Tang Z., Shen S., Atluri S.N. (2003): Analysis of materials with strain-gradient effects: A Meshles Local Petrov-Galerkin (MLPG) approach, with nodal displacements only. *CMES: Computer Modeling in Engineering and Sciences*, 4 (4): 177-196

Verbeek, C. J. R. (2003): The influence of interfacial adhesion, particle size and size distribution on the predicted mechanical properties of particulate thermoplastic composites. *Mater. Lett.*, vol. 57, pp. 1919-1924.

Wang, J., Lam, D. C. C. (2009). Model and analysis of size-stiffening in nanoporous cellular solids. *J. Mater. Sci.*, vol. 44, pp. 985-991.

Wang, K., Wu, J., Ye, L., Zeng, H. (2003): Mechanical properties and toughening mechanisms of polypropylene/barium sulfate composites. *Compos. Part A-Appl. S.*, vol. 34, pp. 1199-1205.

Wei, W., Lam, D. C. C. (2010): Size-Dependent Behavior of Macromolecular Solids I: Molecular Origin of the Size Effect, *CMES: Computational Modeling in Engineering Sci.*, vol.63, no.1, pp.1-14.

Yang, F., Chong, A. C. M., Lam, D. C. C., Tong, P. (2002): Couple stress based strain gradient theory for elasticity. *Int. J. Solids Struct.*, vol. 39, pp. 2731-2743.

Appendix A: Typical conventional composite elastic modulus models

Model name	Equation	Description
Parallel (Voigt) model	$E_{co} = E_p\varphi_p + E_m(1-\varphi_p)$	Upper bound
Series (Reuss) model	$E_{co} = \frac{E_pE_m}{E_p(1-\varphi_p)+E_m\varphi_p}$	Lower bound
Combing model	$E_{co} = f_c(E_{Voigt} - E_{Reuss}) + E_{Reuss}$, $f_c \in [0,1]$	(Coran, 2000)
Einstein's equation	$E_{co} = (1+2.5\varphi_p)E_m$	(Einstein and Fürth, 1956)
Guth's equation	$E_{co} = \left(1+2.5\varphi_p+14.1\varphi_p^2\right)E_m$	(Guth, 1945)
Counto's equation	$\frac{1}{E_{co}} = \frac{1}{E_m}\left(\frac{1}{E_p/E_m+\varphi_p^{-1/2}-1}+1-\varphi_p^{1/2}\right)$	(Counto,1964)
Kerner's equation	$\frac{E_{co}}{E_m} = 1+\frac{\varphi_p}{1-\varphi_p}\frac{15(1-\nu_m)}{(8-10\nu_m)}$	(Kerner,1956)

Appendix B Molecular rotations in strained solids with non-negligible strain gradients

Macromolecules deform by molecular rotations. The details are shown in Fig. B1. In the figure, the deformation is illustrated using a simple cross-linked polyethylene molecules embedded in a beam shown in the subfigure (a). The change in stiffness is shown in (b) as a function of beam thickness. When a thick beam is bent, the molecules are strained with little strain gradients at point in subfigure (b). The molecular orientation without strain is shown in (c), and with strain alone is illustrated in (d). The effective elastic modulus is size-dependent owing to additional non-negligible strain gradients when the beam is thin. The molecular behavior under the same strain, but with strain gradients is shown in subfigure (e). The combination of strain and strain gradient results in more rotations and led to an effective increase in the elastic modulus of the polyethylene beam. Since strain gradients between molecules are proportional to the thickness of the beam, additional molecular rotations from strain gradients naturally give rise to size dependence in bending of macromolecular polymeric beams and in deformations where strain gradients are high.

Appendix C FEM verification

The higher-order analytical solutions for pure bending and torsion with rotation gradient have been derived by Yang et al.(2002). The pure bending and torsion solutions are

$$\frac{M}{M_0} = 1 + 6\,(1-v)\left(\frac{l_2}{h}\right)^2 \tag{16}$$

and

$$\frac{Q}{Q_0} = 1 + 6\left(\frac{l_2}{r}\right)^2 \tag{17}$$

respectively, where M_0 and Q_0 are conventional moment and torque respectively; M and Q are moment and torque with higher-order effect; h is the bending beam thickness; r is the torsion rod radius; v is the Poisson's ratio. Using displacement template method, the 2-D 8-node and 3-D 20-node higher-order elements were used to model the higher-order deformation behavior in pure bending and torsion, respectively. The FEM results are compared with analytical solutions in Fig. C^1 and are in good agreement with analytical solutions.

The cantilever bending experiments of epoxy thin beam was carried out by Lam et al.(2003). The rising of bending rigidities with decreasing of beam thicknesses

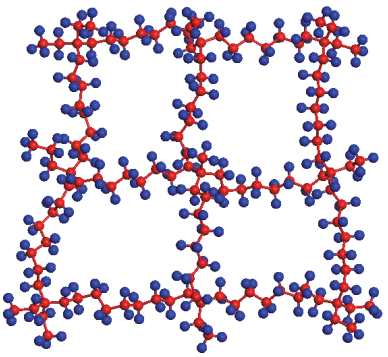

(a) Molecular model

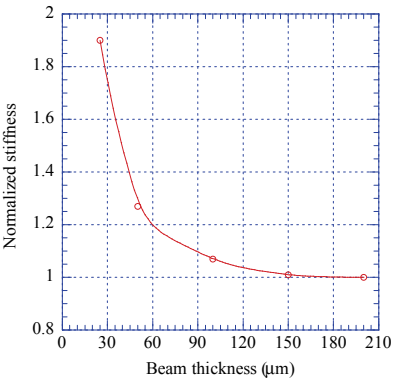

(b) Thickness dependence

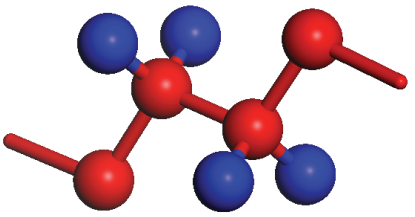

(c) Unstrained

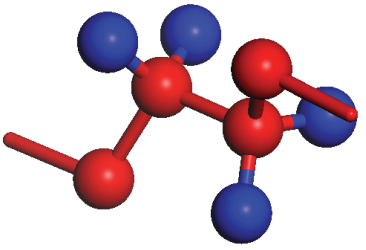

(d) Strained

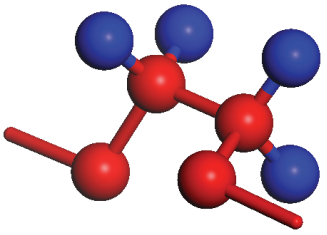

(e) strained with strain gradients

Figure B1: The geometric necessary rotation on molecular level.

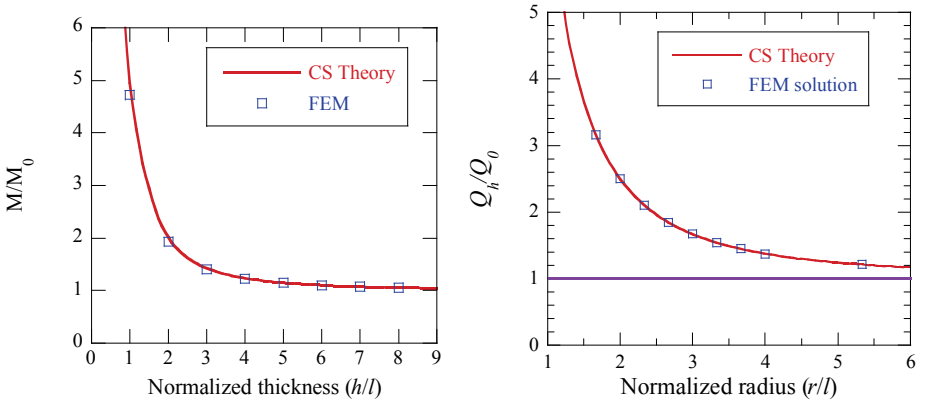

(a) pure bending case (b) torsion case

Figure C1: Comparison of FEM and analytical solutions for pure bending and torsion.

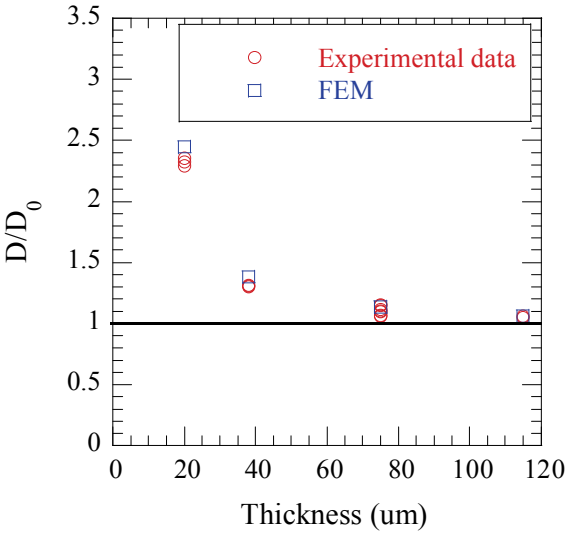

Figure C2: Comparison of the normalized rigidity from experiments (Lam et al., 2003) and FEM results. D and D_0 are beam rigidity with/without higher-order effect.

were found in the experiments. With the higher-order FEM analysis, the results of normalized bending rigidities varied with beam thickness are compared in the Fig. C2. The good agreement between FEM and experimental results are achieved.